Anal. Methods Environ. Chem. J. 7 (2) (2024) 59-73

AMECJ

Research Article, Issue 2
Analytical Methods in Environmental Chemistry Journal
Journal home page: www.amecj.com/ir

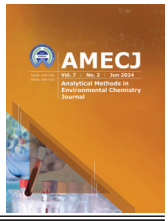

Synthesis-activated carbon based on various agri-food wastes for highly efficient removal of an anionic dye before analysis by UV-Vis spectrometry

Mohamed Ennabely [a,*], Abdessamad Ouedrhiri[a], Youssef Lghazi[a], Boubaker Youbi[a], Abderrafie Kettani Halabi [a], Mostafa Khoukhi [a], and Itto Bimaghra[a]

[a]*Bio-Geosciences and Materials Engineering Laboratory, Ecole Normale Superieure, Hassan II University of Casablanca, Morocco*

ARTICLE INFO:

Received 16 Feb 2024
Revised form 20 Apr 2024
Accepted 18 May 2024
Available online 29 Jun 2024

Keywords:
Analytical method
Activated carbons
Adsorption
MB-Dye
Agricultural-food wastes
UV-Vis spectrometry

ABSTRACT

This study aims to valorize three agricultural-food (agri-food) wastes: Argan husks, dates seeds, and olive stones collected from various regions of Morocco to produce three types of activated carbons (ACah),(ACds) and (ACos) respectively. These activated carbons were used to compare their effectiveness in removing methyl orange, an organic pollutant in aqueous solutions. The precursor materials were carbonized at a temperature of T=900°C for 2 hours and subsequently chemically activated using phosphoric acid (H_3PO_4) in a weight ratio of 1:2. The obtained samples were characterized by Fourier-transform infrared spectroscopy (FTIR), scanning electron microscopy (SEM), and BET-analysis to determine the specific surface area. The analysis revealed that (ACah) displayed a rough surface with more pores and O-H chemical bonds, indicating its superior adsorption properties. This finding corresponds to the BET-specific surface areas obtained, which were 476 m^2g^{-1} for ACah, 441 m^2g^{-1} for ACds, and 362 m^2g^{-1} for ACos. In all methyl orange adsorption experiments (10 mg L^{-1}), 60 mg of each activated carbon was used for 30 minutes, resulting in removal efficiencies of 93.87% for ACah, 91.83% for ACds, and 89.79% for ACos. The examination of adsorption kinetics and isotherm analysis demonstrated a strong alignment of the adsorption data with both the pseudo-second-order and Langmuir models across various materials.

1. Introduction

Undoubtedly, discharging untreated wastewater or aqueous solutions containing chemical pollutants into the environment poses significant risks, potentially harming human health[1] and causing adverse environmental effects[2]. The presence of organic pollutants in the environment can lead to a reduction in dissolved oxygen levels in water[3]. Thus, removing these organic pollutants from aqueous solutions becomes crucial before their release. Our focus in water treatment is to tackle this issue using cost-effective and straightforward methods, such as activated carbon adsorption. This method is highly effective in eliminating organic substances from aqueous solutions[4], the methyl orange (MO, anionic dye, offering the additional benefit of reusing agricultural waste and safeguarding the environment from pollutants. Notably, Morocco generates a substantial volume of agricultural residues annually, including olive stones[5], date seeds[6], and Argan husks[7], which can pose challenges related to aesthetics

*Corresponding Author: Mohamed Ennabely
Email: ennabely.mohamed@gmail.com
https://doi.org/10.24200/amecj.v7.i02.310

and environmental impact. Dyes, particularly MO (methyl orange), are commonly utilized materials in the food, pharmaceutical, printing, and textile industries[8]. Although not extremely toxic, this dye can still have adverse effects on the environment and human health, causing symptoms like an increased heart rate, diarrhea, and imparting an unpleasant color and odor to water bodies[9]. Additionally, it obstructs sunlight, crucial for photosynthesis[10]. Therefore, before releasing solutions containing MO molecules into the environment, treatment is necessary. We aim to achieve this by producing three distinct types of activated carbons: ACah, ACds, and ACos; from Argan husks, date seeds, and olive stones, respectively. Subsequently, we will assess their efficacy in removing the methyl orange molecule from an aqueous solution. This study serves a dual purpose: firstly, it involves the valorization of Argan shells, and secondly, it evaluates the capacity to eliminate the MO dye.

2. Materials and Methods

2.1. Materials

The biomass derived from agricultural waste illustrated in Figure 1 originates from different regions across Morocco. Olive pits were specifically sourced from the olive mill situated in the Settat region, whereas date seeds and argan shells were collected in the Sidi Ifni province. Methyl orange (C.I. No: 13025)[11] was employed as the adsorbate in all experiments. Phosphoric acid (H_3PO_4, molar mass:97.9952 g mol^{-1})[12] was utilized at a concentration of 1 mol L^{-1}, and all procedures were conducted using distilled water.

2.2. Synthesis of activated carbons

A batch of collected waste was cleansed using distilled water to eliminate impurities and then dried at 120°C for 12 hours in an oven. This resultant material underwent a drying, grinding, and sieving process through a sieve with five micrometer pores to yield the untreated raw materials in a powdered state. Subsequently, the carbonization step took place in an oven (PROTERM-PLF 120/6) at 900°C for two hours. The chemical activation process was carried out by mixing the powder with phosphoric acid, maintaining a weight ratio of 1:2. Following this, distilled water was added to the mixture, reaching a volume of 50 ml while being stirred for 10 minutes. The samples were then left for overnight drying at 120°C and subjected to washing, using demineralized water along with sodium hydroxide until neutralization was achieved to delete any remaining residual amounts of acid H_3PO_4. Finally, the activated carbons underwent filtration and further drying at 120°C for 12 hours.

Fig. 1. The three precursors and their activated carbons

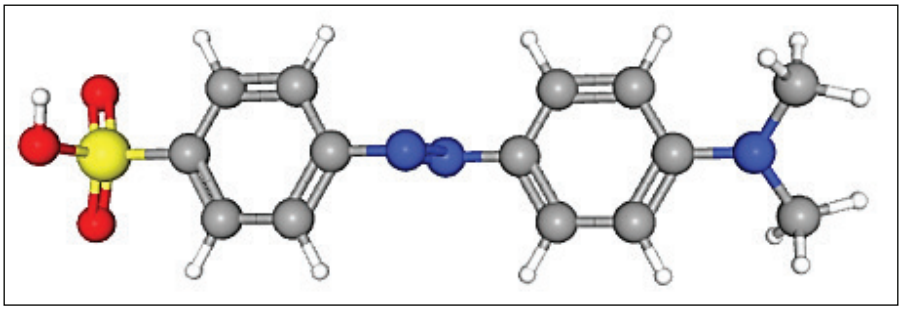

Fig. 2. Three-dimensional molecular model of methyl orange.

2.3. Characterizations of Activated carbons

The physical and chemical properties of the materials utilized are crucial in understanding adsorption behaviors. Fourier transform infrared spectroscopy is one of the most important tools for this purpose because it allows for a qualitative examination of the surface functional groups of ACah, ACds, and ACos. The FTIR analysis was carried out using a TENSOR 27 type spectrometer (Bruker Company, Germany) for three samples obtained by mixing 100 mg of potassium bromide with 1 mg of each activated carbon, the data was recorded in the 4000-500 cm^{-1} range plot IR spectra. Scanning Electron Microscopy (SEM) of three activated carbons has been performed with an Energy Dispersive Spectrometer using a Philips XL 30FEG with a secondary electron detector (SE) and an electron acceleration voltage of 20 kV. Also, our activated carbons' BET surface area was ascertained by N_2 adsorption-desorption measurements using an automated Micromeritics system running at 77 K.

2.4. Adsorption Procedure

MO-dye, also recognized as Sodium-4-(4-dimethylamino phenyl diazenyl), represents an anionic dye[13] ($C_{14}H_{14}N_3SO_3Na$) dissolved in distilled water for its preparation. The reason behind its absorption of light within the visible spectrum lies in the dye molecule's extensive conjugated system. Its absorption spectrum demonstrates a peak at λmax = 465 nm, as determined by a UV-Vis spectrophotometer (UV-1800, Bejing Rayleigh Co. Ltd). This particular wavelength corresponds to the color that complements yellow-orange, thus justifying the name "methyl orange." The optimized three-dimensional structure depicted in Figure 2 was obtained via the Gaussian program. Equation (1) is utilized to compute the adsorption percentage (R%) of methyl orange, using the initial absorbance value A0 and the final absorbance value A1 [14] The quantity qe (mg/g) of methyl orange adsorbed onto the treated material can be determined using Equation (2)[15]. The methyl orange concentration was determined by the UV-Vis spectrophotometer and the relationship between absorbance for the methyl orange is illustrated in Figure 3.

$$\mathbf{R\%} = \frac{\mathbf{A0-A1}}{\mathbf{A0}} * 100 \qquad \text{(Eq.1)}$$

$$\mathbf{q_e} = \frac{\mathbf{V(C_0 - C_e)}}{\mathbf{M}} \qquad \text{(Eq. 2)}$$

The variables included in this equation are as follows:
C_0 denotes the initial concentration of MO-dye (mg L^{-1})
C_e stands for the equilibrium concentration of the MO-dye (mg L^{-1})
V represents the volume of the solution (L)
M denotes the mass of the adsorbent (g)

The instrument employed for UV-Vis spectrometry utilizes a UV-Vis spectrophotometer, measuring absorbance across specific wavelengths [16]. This high-sensitivity equipment enables precise quantification of sample concentrations. Calibration curves were generated to correlate absorbance with concentration, ensuring accurate analyses. The instrument's capabilities enhance the study's capacity for investigating molecular absorption characteristics with increased precision.

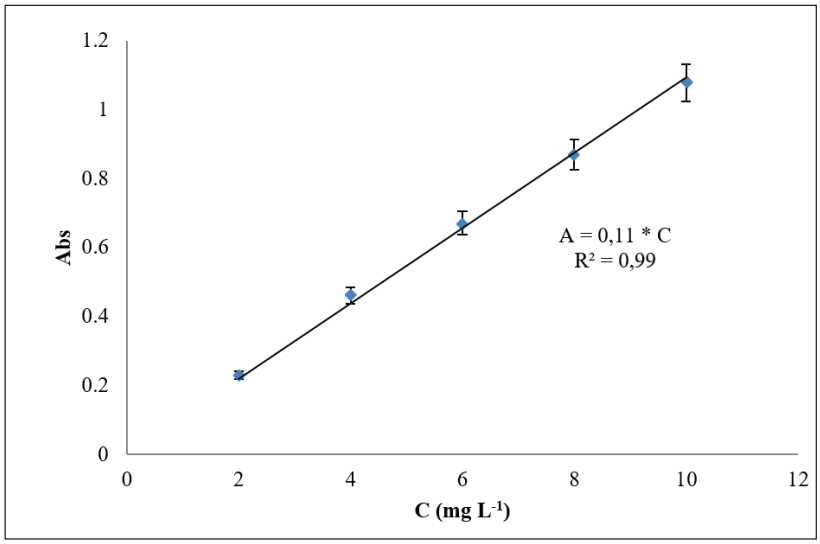

Fig. 3. Concentration versus absorbance (abs) for methyl orange by the UV-Vis spectrophotometer

3. Results and discussions

3.1. FTIR-analysis

Figure 4 displays the FTIR spectra of the three adsorbents. These spectra reveal unique properties for each material. Due to the stretching vibration of the hydroxyl groups produced by the O-H bond, ACah exhibits a distinct and broadband at about 3405 cm^{-1}[17]. The ACds exhibit a peak around 1101 cm^{-1}, which corresponds to the presence of C-O groups in secondary alcohol groups[18]. The ACos, shows a distinct peak at approximately 1475 cm^{-1}, indicating C-H vibrations within the methylene linkage. Additionally, there are peaks at 1051 cm^{-1}, signifying C-O vibrations related to oxygen-containing groups[19].

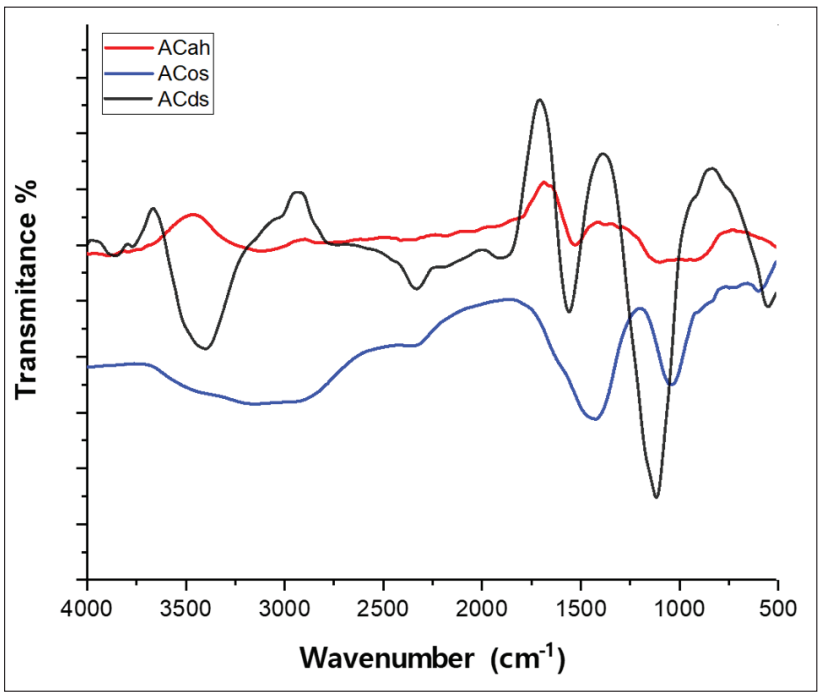

Fig. 4. FTIR-spectra of ACah, ACds, and ACos adsorbents

Figure 4 illustrates numerous peaks, indicating several functional groups existing on the surface of our adsorbents. These groups actively participate in the adsorption of MO, primarily due to the distinct O-H stretching vibration observed specifically on the ACah surface. This phenomenon could be the key reason behind the strong attraction of MO molecules through electrostatic forces[20]. Nevertheless, the presence of the C-O group on the surfaces of ACds and ACos can slow down the adsorption process. This disparity might provide an explanation as to why ACah functions as a more effective adsorbent compared to the others.

3.2. SEM analysis

The SEM images presented in Figure 5 reveal the structural and morphological characteristics of ACah, ACds, and ACos. It is clear that the rough texture of the ACah surface, which has many small-diameter pores, makes it unique. This porous structure provides an abundance of adsorption sites for the dye, making it well-suited to the size of the MO molecule. This promotes the dye's penetration into the material and raises the possibility of adsorption. Whereas ACos has a rough surface with thin layers and granules that may improve the physical adsorption of MO[21], ACds have an uneven surface structure with micropores. As shown in Table 1, the specific surface areas (SSA) of our adsorbents are also calculated using the BET analysis method. Compared to the other two adsorbents under study, ACah has a noticeably larger specific surface area, per the data in Table 1. The reason for the higher adsorption efficiency of ACah compared to the other two adsorbents can be better understood with the aid of all these observations.

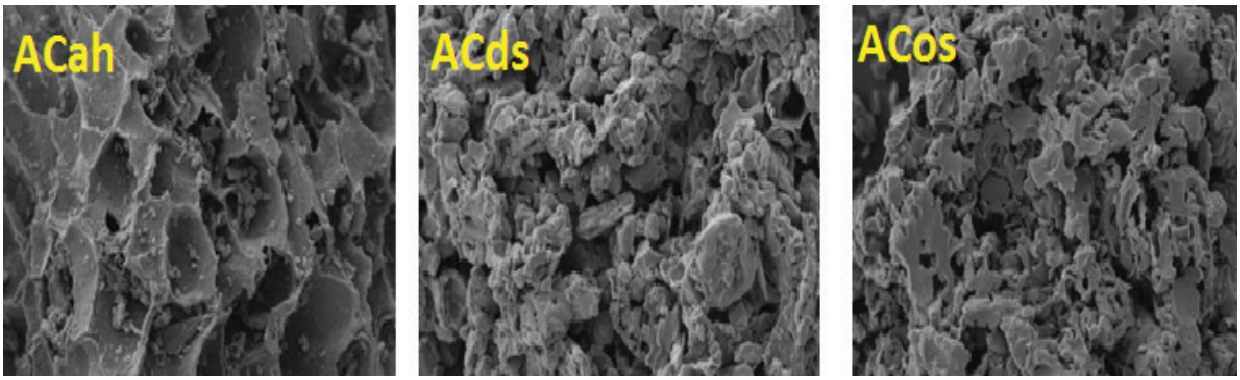

Fig. 5. SEM-images of ACah, ACds, and ACos adsorbents

Table 1. BET values for ACah, ACds, and ACos.

SSA	ACah	ACds	ACos
BET (m^2 g^{-1})	476	441	362

3.3. Adsorption Studies

3.3.1. Contact time effect

Figure 5 displays the results obtained from experiments investigating the impact of varying contact time duration on the adsorption process aiming to determine the quantities of methyl orange (MO) removed from a 25 mL solution with a concentration of 10 mg L^{-1}. The adsorption process utilized 0.06 grams of three distinct adsorbents: ACah, ACds, and ACos. The experiments encompassed contact times ranging from 5 to 30 minutes while ensuring a constant stirring speed of 500 rpm.

Two separate stages are shown in Figure 6. At the beginning of the experiment, the adsorption process moves rather quickly. The high accessibility of active empty sites on the surface of ACah, ACds, and ACos, could be the reason for this. But once 20 minutes pass, there is a slower phase that is noticed. Because there is a tendency for these active empty sites to become less available for MO molecule binding[22] this slower phase is thought to be the most optimal one. We also measured the removal efficiency, which can reach 93.87% for ACah, 91.83% for ACds and 89.79% for ACos. This high efficiency is due to the microporous structure of the materials. Based on these results, we can conclude that the activated carbon of Argan husks stands out as the superior adsorbent for methyl orange dye in comparison to the other two precursors. These findings align with the BET values acquired and listed in Table 2.

3.3.2. MO-concentration effect

Five specimens were created, each holding 25 milliliters of MB solution at concentrations of 2, 4, 6, 8, and 10 mg L^{-1}, they were mixed at 500 rpm for 20 minutes, and 0.06 g of each adsorbent ACah, ACds, and ACos. were added to each sample. This experiment was designed to evaluate the effects of adsorbate concentration on the adsorption process. Figure 7 illustrates the results obtained.

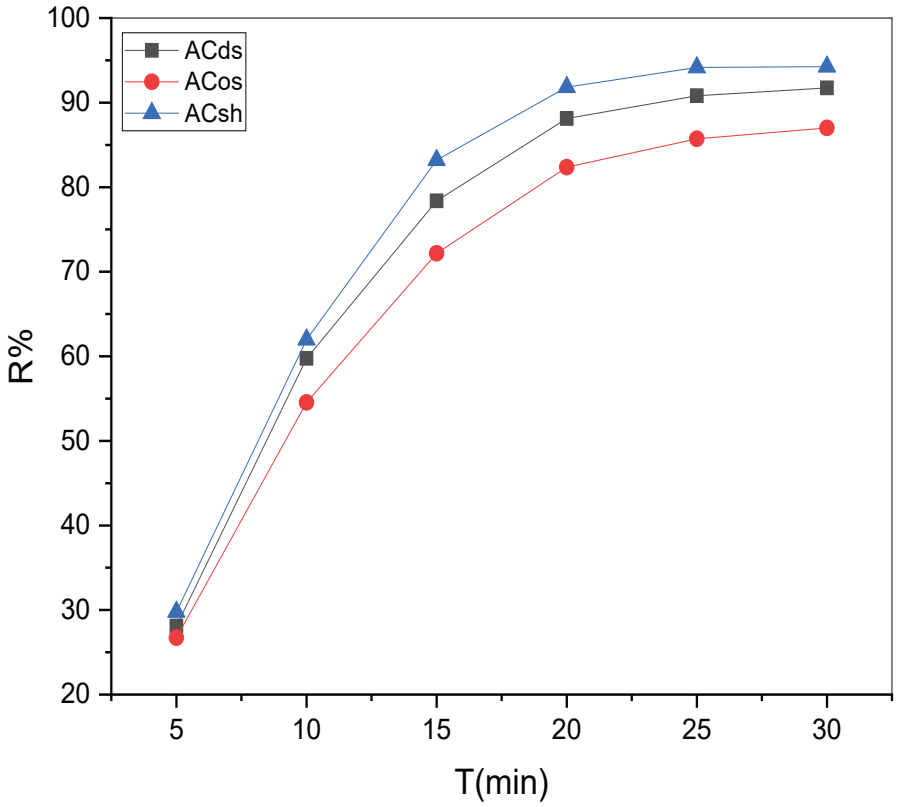

Fig. 6. The recovery of MO removal as a function of t (min) for ACah, ACds, and ACos adsorbents

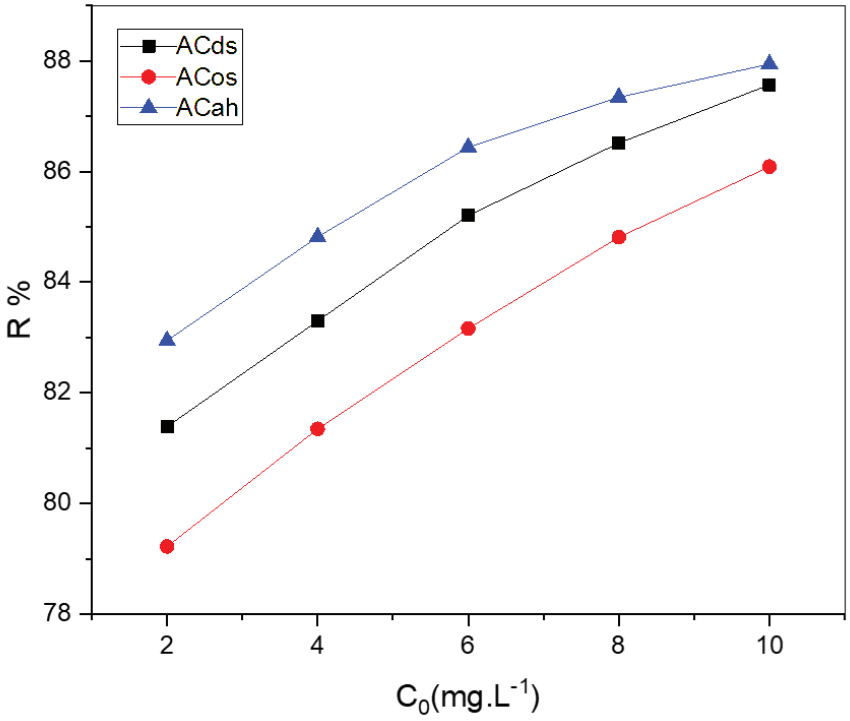

Fig. 7. The effect of MO concentration on removal efficiency(%R)

As the concentration rises, the rate of MO removal also increases, as indicated by the data presented in Figure 7. This implies that a significant proportion, if not nearly all, of the pores are nearly completely occupied. Among the adsorbents tested, ACah continues to stand out as the most effective adsorbent for MO dye, with a percentage difference of approximately 8%.

3.3.3.Effect of temperature

The study examined how altering temperatures between 20°C and 60°C affected the adsorption processes. The experimental conditions included consistent parameters: a fixed volume (V) of 25 mL, an initial concentration (C) of 10 mg L^{-1}, a pH maintained at 7.3, a reaction time of 20 minutes, agitation at 500 rpm, and an adsorbent mass of 0.06 g, Figure 8 displays the findings obtained from these tests.

We observe that when the temperature rises, MO's adsorption capacity on ACah, ACds, and ACos decreases. The adsorption process exhibits an exothermic nature as confirmed by these observations, this gives negative values for standard enthalpy ($\Delta H<0$)[23]. The reverse adsorption process, which begins at a temperature of about 30°C, is what causes this decrease in the adsorbed amount. It is essential to comprehend this phenomenon to restore activated carbons. The experimental data presented in the figure suggest that the highest adsorption occurs between 20 and 30°C, which corresponds to room temperature. We were also able to achieve a similar removal percentage of 80% for all three activated carbons at a temperature of around 50°C.

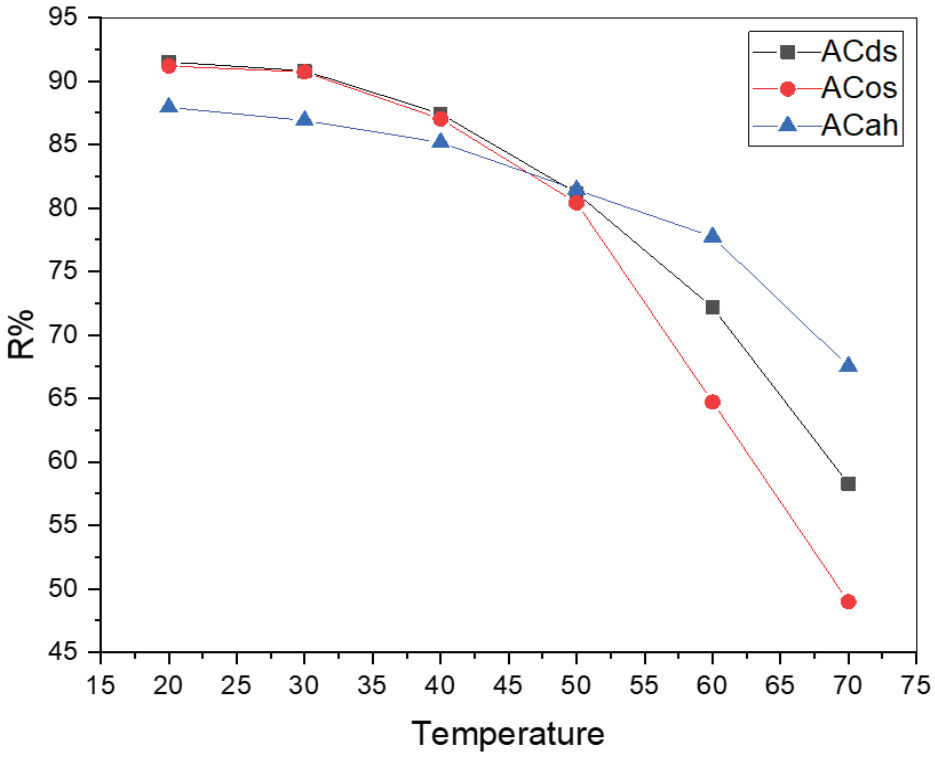

Fig. 8. The impact of temperature on the extent of removal

3.4. Adsorption isotherms

An adsorption isotherm, which generally depicts the adsorption capacity at equilibrium as a function of concentration under particular experimental conditions, can be used to further characterize the adsorption process. The obtained experimental data is used for this. Two of the most commonly used models for fitting experimental adsorption data are the Langmuir and Freundlich models. These models provide parameters that shed light on the mechanisms underlying the adsorption process.

3.4.1.Langmuir Isotherm

To determine the Langmuir isotherm, a graph is constructed by plotting 1/qe as a function of 1/Ce, as depicted in Figure 9. The linear representation of this relationship is expressed by Equation 3. In this Equation, qe signifies the quantity of adsorbed dye, Ce represents the equilibrium concentration of the adsorbate, Qm indicates the maximum adsorption capacity observed during the reaction, and K denotes the Langmuir constant[24]. The plot Figure 9 shows a straight line with $q_{(max)}$ and *kL* determined from the y-intercept and slope, respectively, with a correlation factor of 0.99 for all three materials confirming the validity of the Langmuir model.

$$\frac{1}{qe} = \frac{1}{Qmax} + \frac{1}{K.qmax}.\frac{1}{Ce}$$

(Eq. 3)

3.4.2.Freundlich isotherm

The Freundlich adsorption isotherm is an empirical relationship describing the connection between the adsorbed amount (qe) and the concentration (Ce) of a solute adsorbed on the surface. The experimental findings demonstrate a direct relationship between the concentration and the adsorption of the adsorbate as illustrated in Figure 10. This relationship can be established by graphing the natural logarithm of qe against the natural logarithm of Ce and is represented by the linear form of the Freundlich Equation (4), with the constants KF indicating the capacity of adsorption and (n^{-1}) representing the intensity of adsorption [25].

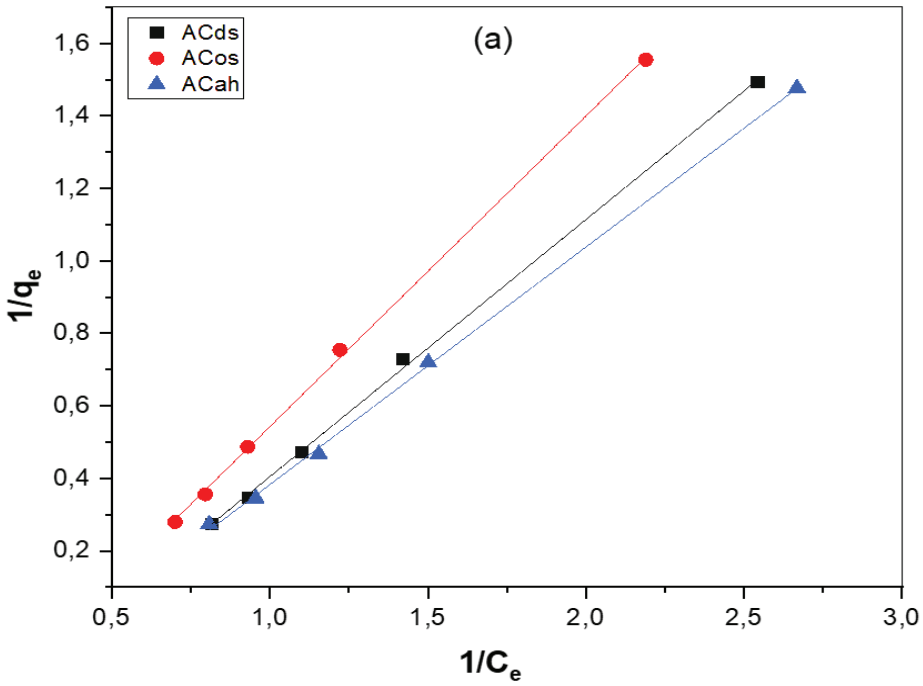

Fig. 9. Isotherm of Langmuir (a) for MO-adsorption on ACah, ACds, and ACos

$$\mathbf{Ln(qe)} = \mathbf{Ln(KF)} + \frac{\mathbf{1}}{\boldsymbol{n}}.\mathbf{Ln(Ce)}$$

(Eq. 4)

k_F and n are the Freundlich constants for adsorption capacity and adsorption intensity, derived from the linear plot in Figure 10 and listed in Table 2. The Freundlich's parameters, n, and KF, as well as the Langmuir parameters, KL and Qm, were determined after the previous adsorption isotherm analysis. These results are listed in Table 2.

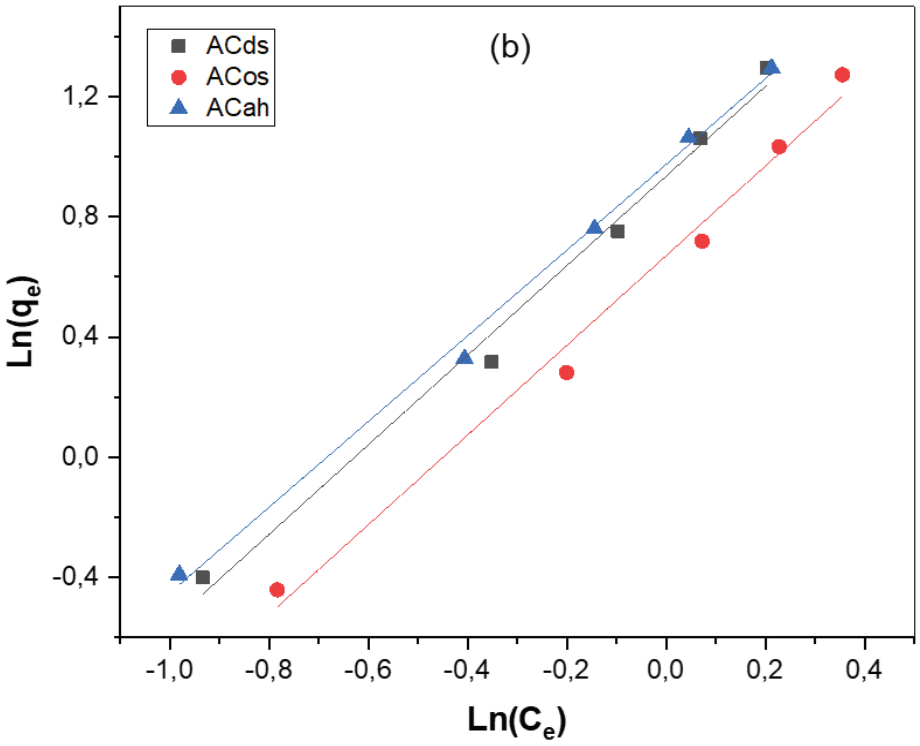

Fig. 10. Isotherm of Freundlich(b) for MO-adsorption on ACah, ACds, and ACos

The Langmuir equation yielded higher correlation coefficients (R^2> 0.99) compared to other models. This indicates that the Langmuir equation is a favorable choice for fitting the experimental adsorption data, enabling the evaluation of the maximum adsorption capacities of the adsorbate on the three adsorbents. Figure 11 offers a comparative examination of the maximum adsorption capacities of MO dye on the three activated carbons used ACah, ACds, and ACos, and Langmuir's Qmax, K_L were determined and listed in Table 3. Within a half-hour of contact time, the maximum adsorption capacities for ACah, ACds, and ACos are recorded as 3.67 mg g^{-1}, 3.27 mg g^{-1}, and 3.19 mg g^{-1}, respectively, as depicted in Figure 11. This indicates that, in comparison to the other two adsorbents, ACah demonstrates the most efficient removal of MO dye. To assess the performance of the material obtained, the adsorption capacity found in this study was compared with other results available in the literature dealing with the adsorption of methyl orange (Table 3**).** Also, many nano adsorbents such as activated carbon, carbon nanotubes, carbon quantum dots, fullerene nanoparticles, and graphene were used for the removal of organic material in different matrixes [26-29]. This comparison more or less confirms that agricultural waste can be considered a precursor to activated carbon, which is used effectively as an adsorbent for toxic dyes at low concentrations.

Table 2. Freundlich and Langmuir adsorption isotherm parameters of MO adsorbed by ACah, ACds, and ACos

Adsorbent	Langmuir parameters			Freundlich parameters		
	Qmax (mgg^{-1})	*K_L (L.mg^{-1})*	*R^2*	*n*	*K_F*	*R^2*
AC ah	3.67	0.43	0,993	0.70	2.65	0,991
AC ds	3.27	0.44	0,991	0.67	2.54	0,981
AC os	3.19	0.37	0,991	0.67	1.95	0,980

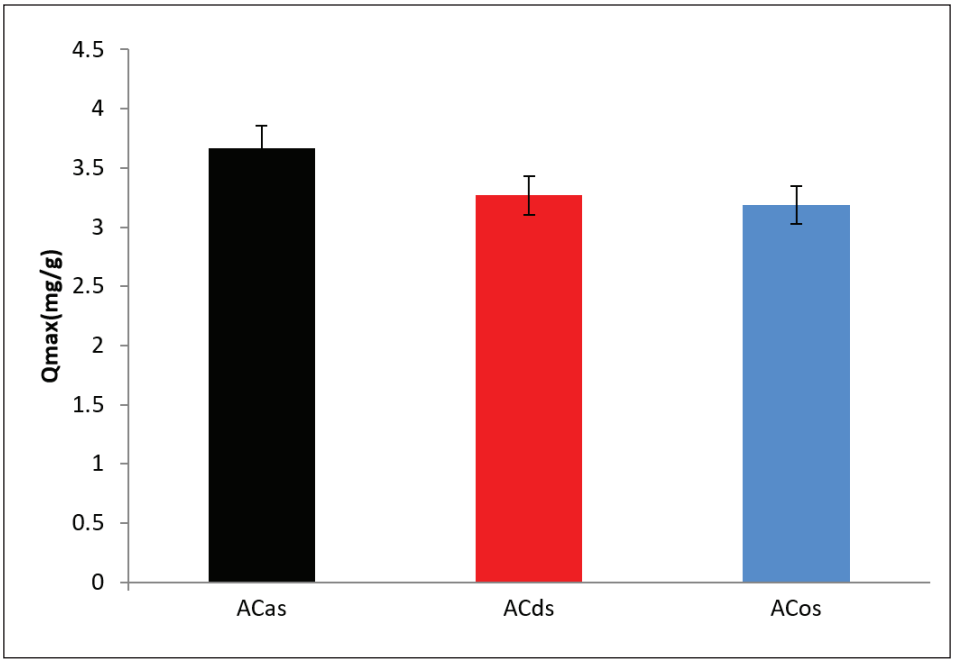

Fig. 11. Adsorption capacities comparison of ACah, ACds, and ACos by Langmuir model

Table 3. Comparison of adsorption capacity (mg g^{-1}) for methyl orange onto ACah, ACds, and ACos with other adsorbents

Adsorbents	qmax (mg g^{-1})	Concentration (mg L^{-1})	pH	T (C°)	Time (min)	Ref.
AHM	15.56	50	6	30	30	[30]
MGGP	16.94	50	3.7	25	60	[31]
N–TiO_2	14.1	21	-	20	300	[32]
ACah	3.67	10	7	25	30	This study
ACds	3.27	10	7	25	30	This study
ACos	3.19	10	7	25	30	This study

AHM: Amino-crosslinked hypromellose
N–TiO_2: Nitrogen-doped–titanium oxide
MGGP: Multigene genetic programming

3.5. Adsorption kinetics

The adsorption rate of the adsorbate is described by kinetic studies. This aspect is crucial in understanding the adsorption process as it directly influences the duration of the adsorption process. This study employed the pseudo-first-order model, pseudo-second-order model, and intraparticle diffusion model to explore the kinetics of adsorption processes and determine the reaction order of MO on three activated carbons: ACah, ACds, and ACos.

3.5.1. The pseudo-first-order model

Equation (5) delineates the pseudo-first-order model, and after a straightforward mathematical integration, it assumes the linear form denoted by Equation (6). In this context, qe and qt represent the quantity of MO adsorbed at equilibrium and at a specific time, respectively, while Kf denotes the pseudo-first-order rate constant[33]. Kinetic is depicted in Figure 12 as a pseudo-first-order for the adsorption of MO onto activated ACah, ACds, and ACos.

$$\frac{dq_t}{dt} = K_1(q_e - q_t) \qquad \text{(Eq. 5)}$$

$$\ln(q_e - q_t) = \ln(q_e) - K1 \times t \qquad \text{(Eq. 6)}$$

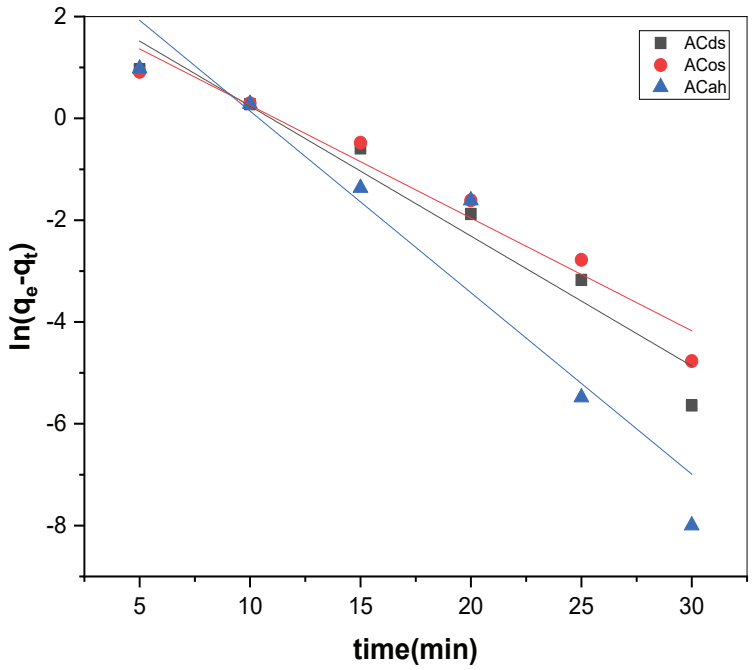

Fig. 12. Pseudo-first order kinetic of MO-adsorption on ACah, ACds, and ACos adsorbents

3.5.2. The pseudo-second-order kinetic model

The pseudo-second-order model is expressed by the differential Equation (7). Upon mathematical integration, Equation (8) is obtained, with K_2 representing the rate constant associated with the pseudo-second-order[34]. Kinetic is depicted in Figure 13, as the second-order for the adsorption of MO onto activated ACah, ACds, and ACos.

$$\frac{dq_t}{dt} = k_2(q_e - q_t)^2 \qquad \text{(Eq.7)}$$

$$\frac{t}{q_t} = \frac{1}{(k_2 q_e^2)} + \frac{1}{q_e}t \qquad \text{(Eq. 8)}$$

Kinetic comparison is depicted in Figure 12 and Figure 13, and the pseudo-first-order and second-order parameters for the adsorption of MO onto activated ACah, ACds, and ACos are detailed in Table 4. The results suggest that the pseudo-second-order model is more suitable than the pseudo-first-order model for studying the adsorption kinetics of MO on the three activated carbons. This preference arises from the pseudo-second-order model's dependence on a longer period, facilitating close or complete adsorption of the adsorbing element. Experimentally, the correlation between the amount of adsorbent and the periods is evident from the curve, with a high coefficient of determination ($R^2 > 0.99$).

4. Conclusions

Three carbonaceous materials such as ACah, ACds, and ACos adsorbents were prepared by activating different precursors with phosphoric acid. They were tested for removal of methyl orange dye in aqueous media. Adsorption rates reached 93.87%, 91.83%, and 89.79% respectively. AC ah can be said to be the most powerful adsorbent, with a slightly higher rate. This is in line with the results of SEM, FTIR, and BET. However, the adsorption of methyl orange onto the three activated carbons is not solely attributed to the pores. It is also influenced by the diverse specific surface areas and the variety of functional groups present on the material surfaces, leading to electrostatic attraction forces.

The isotherm study showed that the Langmuir model proved to be the most appropriate, and the experimental results of the kinetic study corresponded well with the pseudo-second-order kinetic model. As a result, significant efficiencies were achieved

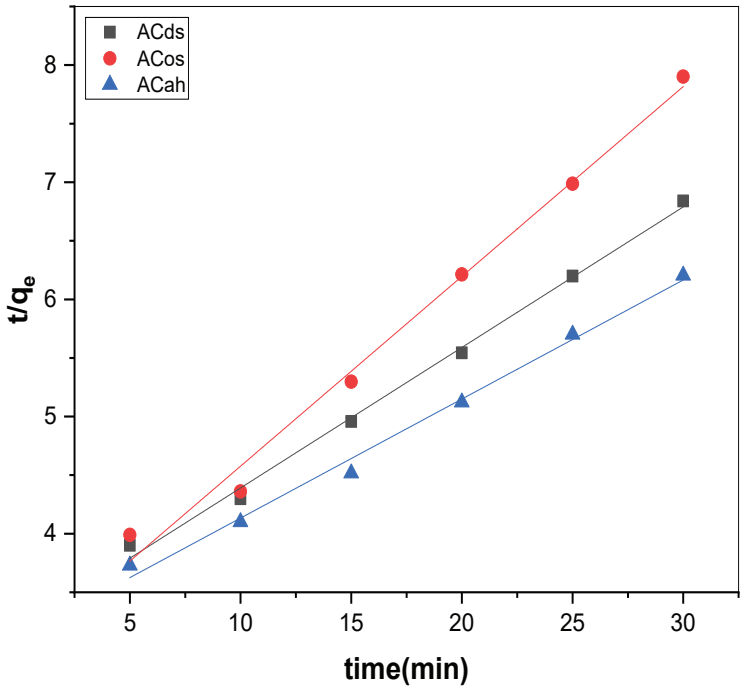

Fig. 13. Pseudo-second-order of MO adsorption on ACah, ACds, and ACos adsorbents

Table 4. Parameters of pseudo-first-order and second-order adsorption of MO on ACah, ACds, and ACos

Adsorbent	Pseudo-first order parameters			Pseudo-second order parameters		
	K_1(1/min)	q_e(mg.g^{-1})	R^2	K_2 (g.mg min^{-1})	qe (m.g^{-1})	R^2
ACah	0.356	8.850	0.911	0.0033	9.840	0.999
ACds	0.255	7.361	0.955	0.0045	8.341	0.991
ACos	0.221	6.121	0.950	0.0001	6.172	0.992

in the removal of a toxic and polluting dye by three activated carbons, with the possibility of regenerating them, this holds significant ecological importance.

5. List of abbreviations

AC	Activated carbon
MO	Methyl orange
ACOP	Activated carbon of olive pomace
ACDP	Activated carbon of date pits
ACAS	Activated carbon of argan shells
FTIR	Fourier-transform infrared
SEM	Scanning electron microscopy
BET	Brunauer-Emmett-Teller
R (%)	The adsorption rate

6. Acknowledgment

This research was carried out at the Laboratory of Research in Bio-Geosciences and Materials Engineering, ENS Casablanca, Morocco. The authors would like to express their gratitude to all those who contributed to the characterization analyses.

7. References

[1] R.R. Karri, G. Ravindran, M.H. Dehghani, Chapter 1 - Wastewater—Sources, Toxicity, and their consequences to human health, Soft Computing Techniques in Solid Waste and Wastewater Management, Elsevier, pp. 3–33, 2021. https://doi.org/10.1016/B978-0-12-824463-0.00001-X

[2] S. Garg, Z.Z. Chowdhury, A.N.M. Faisal, N.P. Rumjit, P. Thomas, Impact of Industrial Wastewater on Environment and Human Health, in: S. Roy, A. Garg, S. Garg, T.A. Tran (Eds.), Advanced Industrial Wastewater Treatment and Reclamation of Water: Comparative Study of Water Pollution Index during Pre-Industrial, Industrial Period and Prospect of Wastewater Treatment for Water Resource Conservation, Springer International Publishing, Cham, pp. 197–209, 2022. https://doi.org/10.1007/978-3-030-83811-9_10

[3] C. Zhao, L. Meng, H. Chu, J.-F. Wang, T. Wang, Y. Ma, C.-C. Wang, Ultrafast degradation of emerging organic pollutants via activation of peroxymonosulfate over Fe3C/Fe@N-C-x: Singlet oxygen evolution and electron-transfer mechanisms, Appl. Catal. B: Environ., 321 (2023) 122034. https://doi.org/10.1016/j.apcatb.2022.122034

[4] A. Ouedrhiri, M. Ennabely, Y. Lghazi, M. Chafi, S. Alougayl, B. Youbi, A.K. Halabi, M. Khoukhi, I. Bimaghra, Adsorption of anionic and cationic dyes in aqueous solution by a sustainable and low-cost activated carbon based on argan solid waste treated with H3PO4, Environ. Sci. Pollut. Res., (2023). https://doi.org/10.1007/s11356-023-26550-z

[5] A.A. Mana, A. Allouhi, K. Ouazzani, A. Jamil, Feasibility of agriculture biomass power generation in Morocco: Techno-economic analysis, J. Clean. Prod., 295 (2021) 126293. https://doi.org/10.1016/j.jclepro.2021.126293

[6] M.H. Sedra, Date Palm Status and Perspective in Morocco, in: J.M. Al-Khayri, S.M. Jain, D.V. Johnson (Eds.), Date Palm Genetic Resources and Utilization: Volume 1: Africa and the Americas, Springer Netherlands, Dordrecht, pp. 257–323, 2015. https://doi.org/10.1007/978-94-017-9694-1_8

[7] B. Moumni, M. Achik, H. Benmoussa, A. Oulmekki, A. Touache, N. El Moudden, M. Charroud, D. Eliche-Quesada, O. Kizinievic, V. Kizinievic, A. Infantes-Molina, G. Gonzalez

Álvaro, F. Guitián Rivera, Recycling argan nut shell and wheat straw as a porous agent in the production of clay masonry units, Constr. Build. Mater., 384 (2023) 131369. https://doi.org/10.1016/j.conbuildmat.2023.131369

[8] A. Onder, H. Ozay, Highly efficient removal of methyl orange from aqueous media by amine functional cyclotriphosphazene submicrospheres as reusable column packing material, Chem. Eng. Process., 165 (2021) 108427. https://doi.org/10.1016/j.cep.2021.108427

[9] M.A. Dutt, M.A. Hanif, F. Nadeem, H.N. Bhatti, A review of advances in engineered composite materials popular for wastewater treatment, J. Environ. Chem. Eng., 8 (2020) 104073. https://doi.org/10.1016/j.jece.2020.104073

[10] Q. Liu, Z. Zheng, X. Yang, X. Luo, J. Zhang, Effect of factors on decolorization of azo dye methyl orange by oxone/natural sunlight in aqueous solution, Environ. Sci. Pollut. Res., 19 (2012) 577–584. https://doi.org/10.1007/s11356-011-0591-4

[11] M. Saeed, A. Mansha, ZnO catalyzed degradation of methyl orange in aqueous medium, Chiang Mai J. Sci., 44 (2017) 1646-1653. https://www.thaiscience.info/journals/Article/CMJS/10987608.pdf

[12] V.I. Pet'kov, E.A. Asabina, A.V. Markin, K.V. Kir'yanov, Calorimetric study of sodium-rich zirconium phosphate, Thermochim. Acta, 403 (2003) 185–196. https://doi.org/10.1016/S0040-6031(02)00656-1

[13] A. Önder, Preparation of cationic composite hydrogel improved by activated carbon and its use in removal of anionic dye, J. Inst. Sci. Tech., 13 (2023) 1902–1915. https://doi.org/10.21597/jist.1243905

[14] V.K. Gupta, D. Pathania, S. Sharma, S. Agarwal, P. Singh, Remediation and recovery of methyl orange from aqueous solution onto acrylic acid grafted Ficus carica fiber: Isotherms, kinetics and thermodynamics, J. Mol. Liq., 177 (2013) 325–334. https://doi.org/10.1016/j.molliq.2012.10.007

[15] H. ait Hmeid, M. Akodad, M. Baghour, A. Moumen, A. Skalli, G. Azizi, A. Anjjar, M. Aalaoul, I. Daoudi, Adsorption of a basic dye, methylene blue, in aqueous solution on bentonite, Mor. J. Chem., 9 (2021) 416-433. https://doi.org/10.48317/IMIST.PRSM/morjchem-v9i3.23303

[16] D. Saetta, K. Buddenhagen, W. Noha, E. Willman, T.H. Boyer, Ultraviolet/visible absorbance trends for beverages under simulated rinse conditions and development of data-driven prediction model, Food Control, 146 (2023) 109530. https://doi.org/10.1016/j.foodcont.2022.109530

[17] G.L. Arueya, T.M. Oyewale, Effect of varying degrees of succinylation on the functional and morphological properties of starch from acha (Digitaria exilis Kippis Stapf), Food Chem., 177 (2015) 258–266. https://doi.org/10.1016/j.foodchem.2015.01.019

[18] M.F. Mohamad Yusop, A.Z. Abdullah, M.A. Ahmad, Malachite green dye adsorption by jackfruit based activated carbon: Optimization, mass transfer simulation and surface area prediction, Diam. Relat. Mater., 136 (2023) 109991. https://doi.org/10.1016/j.diamond.2023.109991

[19] S. Ramola, T. Belwal, C.J. Li, Y.Y. Wang, H.H. Lu, S.M. Yang, C.H. Zhou, Improved lead removal from aqueous solution using novel porous bentonite - and calcite-biochar composite, Sci. Total Environ., 709 (2020) 136171. https://doi.org/10.1016/j.scitotenv.2019.136171

[20] Y.-Z. Wu, J. Xu, H.-X. Li, Y.-H. Tong, Z.-L. Xu, C. Lian, H. Liu, Enhanced steric effect and desolvation process on organic solvent nanofiltration: A mechanism study for removing anionic dyes, Chem. Eng. J., 446 (2022) 137360. https://doi.org/10.1016/j.cej.2022.137360

[21] W. Pan, H. Xie, Y. Zhou, Q. Wu, J. Zhou, X. Guo, Simultaneous adsorption removal of organic and inorganic phosphorus from discharged circulating cooling water on

biochar derived from agricultural waste, J. Clean. Prod., 383 (2023) 135496. https://doi.org/10.1016/j.jclepro.2022.135496

[22] A.A. Alghamdi, A.-B. Al-Odayni, W.S. Saeed, M.S. Almutairi, F.A. Alharthi, T. Aouak, A. Al-Kahtani, Adsorption of azo dye methyl orange from aqueous solutions using alkali-activated polypyrrole-based graphene oxide, Molecules, 24 (2019) 3685. https://doi.org/10.3390/molecules24203685

[23] M. Husaini, B. Usman, M.B. Ibrahim, Kinetic and thermodynamic evaluation on removal of anionic dye from aqueous solution using activated carbon derived from agricultural waste: equilibrium and reusability studies, Appl. J. Environ. Eng. Sci., 9 (2023) 9–138. https://doi.org/10.48422/IMIST.PRSM/ajees-v9i3.40418

[24] K. Singh, S.K. Azad, H. Dave, B. Prasad, D.M. Maurya, M. Kumari, D. Dubey, A.K. Rai, D. Singh, M. Sillanpää, M.P. Sah, K.S. Prasad, A mechanistic insight into chromium (VI) ion adsorption onto pristine, UCB as well as Al-modified Neolamarckia cadamba wood biochar, Biomass Conv. Bioref., (2022). https://doi.org/10.1007/s13399-022-03620-9

[25] H.N. Tran, Improper estimation of thermodynamic parameters in adsorption studies with distribution coefficient K_D (q_e/C_e) or Freundlich constant (K_F): considerations from the derivation of dimensionless thermodynamic equilibrium constant and suggestions, Adsorpt. Sci. Technol., 2022 (2022) e5553212. https://doi.org/10.1155/2022/5553212

[26] M.B.H. Abadi, Air pollution control: The evaluation of TerphApm@ MWCNTs as a novel heterogeneous sorbent for benzene removal from air by solid phase gas extraction, Arab. J. Chem., 13 (2020) 1741-1751. https://doi.org/10.1016/j.arabjc.2018.01.011

[27] M. Osanloo, Nobel method for toluene removal from air based on ionic liquid modified nano-graphene, Int. J. Occup. Hyg., 6 (2014) 1-5. http://ijoh.tums.ac.ir

[28] C. Jamshidzadeh, A new method for removal of hazardous toluene vapor from air based on ionic liquid-phase adsorbent, Int. J. Environ. Sci. Technol., 16 (2019) 2797-2808. https://doi.org/10.1007/s13762-018-1975-5

[29] C. Jamshidzadeh, A new analytical method based on bismuth oxide-fullerene nanoparticles and photocatalytic oxidation technique for toluene removal from workplace air, Anal. Methods Environ. Chem. J., 2 (01) (2019) 73-86. https://doi.org/10.24200/amecj.v2.i01.55

[30] W. Qu, D. He, H. Huang, Y. Guo, Y. Tang, R.-J. Song, Characterization of amino-crosslinked hypromellose and its adsorption characteristics for methyl orange from water, J. Mater. Sci., 55 (2020) 7268–7282. https://doi.org/10.1007/s10853-020-04517-6

[31] N. Kütük, S. Arslan, Biosorption of methyl orange from aqueous solution with hemp waste, investigation of isotherm, kinetic and thermodynamic studies and modeling using multigene genetic programming, Chem. Papers, 76 (2022) 1–16. https://doi.org/10.1007/s11696-022-02411-w

[32] J. Fan, Z. Zhao, W. Liu, Y. Xue, S. Yin, Solvothermal synthesis of different phase N–TiO_2 and their kinetics, isotherm and thermodynamic studies on the adsorption of methyl orange, J. Colloid Interface Sci., 470 (2016) 229–236. https://doi.org/10.1016/j.jcis.2016.02.045

[33] A. Ouedrhiri, Y. Lghazi, J. Bahar, M. Ait Himi, C. El Haimer, B. Youbi, M. Khoukhi, Y. Bimaghra, Adsorption of the methylene blue dye in environmental water samples by biochar obtained from the valorization of argan shells, Phys. Chem. Res., 10 (2022) 301–313. https://doi.org/10.22036/pcr.2021.303554.1968

[34] E.D. Revellame, D.L. Fortela, W. Sharp, R. Hernandez, M.E. Zappi, Adsorption kinetic modeling using pseudo-first order and pseudo-second order rate laws: A review, Clean. Eng. Technol., 1 (2020) 100032. https://doi.org/10.1016/j.clet.2020.100032